Colloid Polym Sci (2005) 283: 486–495
DOI 10.1007/s00396-004-1199-8

S. Henning
G. H. Michler
F. Ania
F. J. Baltá-Calleja

Microhardness of α- and β-modified isotactic polypropylene at the initial stages of plastic deformation: analysis of micromechanical processes

Received: 27 February 2003
Accepted: 12 July 2004
Published online: 1 December 2004

S. Henning · G. H. Michler (✉)
Institute of Materials Science,
Martin-Luther-Universität
Halle-Wittenberg, 06099 Halle/Saale,
Germany
E-mail: michler@iw.uni-halle.de
Tel.: +49-3461-462745
Fax: +49-3461-462535

F. Ania · F. J. Baltá-Calleja
Instituto de Estructura de la Materia,
CSIC, Serrano 119, 28006 Madrid,
Spain

Abstract The microindentation hardness, H, of uniaxially deformed isotactic polypropylene samples was determined near the neck region, as a function of the draw ratio. The microhardness technique appears to be a valuable tool to describe mechanical properties in localized regions within a material and is capable of following changes in the semicrystalline structure during deformation. Differences in the microhardness behaviour of the two types of polymorphic forms, α and β, of isotactic polypropylene are discussed in terms of the two specific types of morphology, i.e. the cross-hatched arrangement of the crystalline lamellae for the α form and the parallel lamellar stacking for the β form. The changes of H as a function of λ are shown to be in accordance with the transformation in the neck from the spherulitic into the fibre structure. The steep H-decrease observed in the neck region is discussed in the light of the nanomechanical processes as revealed by scanning electron microscopy. These include lamellar separation, microvoid formation and fibrillation. Finally, microindentation experiments carried out in the neck allow an estimation of the local draw ratio at which the maximum pore content in the polypropylene samples occurs.

Keywords Polypropylene · α- and β-modification · Toughness · Microhardness · Porosity · Micromechanics · Electron microscopy

Introduction

Polypropylene (PP) is still one of the most promising polymers for the new demanding technical applications, such as the automotive industry [1–3]. The reason is the versatility of PP, as its structure and properties (including processability) can be tailored to specific requirements. The improvement of the mechanical properties has to be based on a detailed understanding of the micromechanical deformation processes that are closely related to the actual morphology [4–7]. Investigations on the deformation mechanism of PP have been carried out in the past [8]. One of the main goals at present is the enhancement of the toughness, especially at lower temperatures, which is relevant for many outdoor applications.

It is well known that isotactic polypropylene (iPP) exhibits various crystal modifications. The presence of one or more polymorphic forms in iPP is strongly dependent on crystallization conditions (crystallization temperature, cooling rate, pressure, and others [2]). β-Form spherulites (hexagonal iPP) are sporadically observed as singularities embedded in a texture dominated by spherulites of the α-form under certain conditions. By using nucleating agents, pure β-phase can be obtained [2, 9, 10]. iPP samples with predominant β-phase may also be produced at defined crystallization temperatures or by crystallization in a temperature

gradient [11]. Several authors have reported for iPP a strain-induced transition from the β to the α phase, or to a so-called "condis" (conformationally disordered) form [12, 13]. It is known that the β-form of isotactic PP shows an enhanced toughness and impact strength at room temperature (23 °C), even at lower temperatures where a neat PP tends to become very brittle [14–16]. Furthermore, the micromechanical mechanisms responsible for the changes in the mechanical properties of a neat β-iPP are different from the processes known for a neat α-iPP [17–20]. Microvoid formation [21], for instance, plays a key role not only in the explanation of the mechanical behaviour but also in obtaining microporous materials with defined pore sizes and pore content.

Microindentation hardness is emerging in recent years as a rather simple and non-destructive experimental technique that can be applied for the characterization of amorphous and crystalline polymers [22–25], as well as, to polymer blends [26]. In particular, microhardness, H, is very sensitive to changes in the structure of partially crystalline polymers such as PE, PET, PP, and others [22]. Specifically, polyethylene (PE) is one of the materials that have been most intensively studied using the microindentation technique. It has been shown that hardness of PE does not only depend on the crystallinity, but also on the structure of the crystalline domains (e.g., thickness of lamellae), their arrangement and their connection by tie molecules and entanglements in the amorphous layers [27, 28]. It was demonstrated that strain hardening occurring in highly oriented semicrystalline PE could be measured by microindentation, the hardness values and the indentation anisotropy increasing with increasing draw ratio. Furthermore, the change of H with increasing draw ratio was shown to support the transformation from the spherulitic to the fibre structure according to Peterlin's model [5, 27]. Microhardness measurements can also be useful to detect polymorphic transitions in semicrystalline polymers [22]. Microhardness additionally offers the possibility to select local regions of interest within the sample allowing to follow the micromechanical processes and phase transitions induced by a previous deformation. For PP, a hardness increase was observed in the plastic zone of a deformed β-iPP sample which has been ascribed to the strain induced β-to-α polymorphic transition [29].

The aim of the present study is to examine the main differences in the deformation behaviour of the α and β forms of iPP at ambient temperature (23 °C) by using the microindentation hardness method. Attention has been focused on changes of microhardness at the initial stages of deformation. Experimental microhardness data have been related to structural changes of the original lamellar morphology and to the micromechanical mechanisms in the material as revealed by scanning electron microscopy (SEM).

Experimental

Materials

Polypropylene samples were prepared from two high molecular weight commercial iPP grades (BOREALIS AG): α-iPP was Daplen BE50 [30] and β-iPP was Daplen BE60 [31]. Sheets of a thickness of 1 mm were produced using a hot press and subsequent multistage crystallization procedure in the second β-iPP case. Miniaturized, dumbbell-shaped tensile bars were punched out of the plates using a special pierce tool.

Mechanical testing

A MINIMAT miniature materials testing device (Polymer Laboratories, UK) was used to perform tensile deformation experiments at a cross-head speed of 1 mm/min at room temperature. The plastic deformation of the tensile bars of both PP types under load proceeds through formation and propagation of two necks in opposite directions. Stress–strain diagrams were recorded to follow the states of deformation qualitatively (Fig. 1). They will not be discussed in detail in this work because they represent single events and the experiments do not follow any standard specification.

Microhardness measurements

In order to obtain a co-planar geometry and flat surfaces, the deformed samples were epoxy embedded, and microtomed down to the middle section of the tensile bar using a LEICA microtome with a metal blade (Fig. 2). The surface effects (skin morphology or scratches) were thus eliminated. For the microindentation

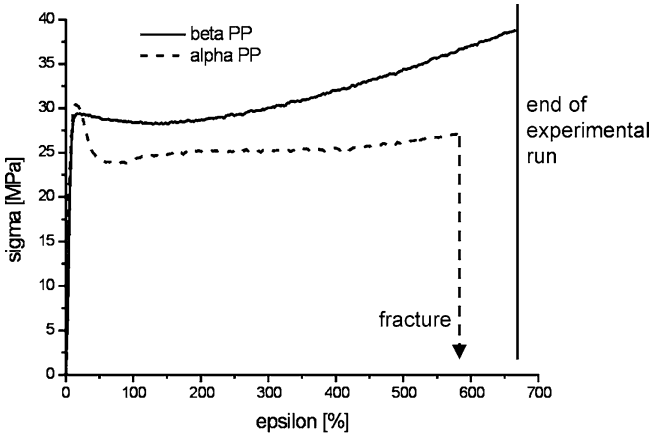

Fig. 1 Stress–strain curves from miniaturized tensile bars of the α-iPP and β-iPP materials

experiments the region corresponding to the different states of deformation, i.e., before, at and directly behind the necking region and after cold drawing, was selected (Fig. 2).

Microhardness measurements were performed at room temperature using a Leitz microhardness tester equipped with a Vickers square pyramidal diamond indenter (168°). Indentation experiments were performed using a load of 98.1 mN and a loading time of 0.1 min. The final permanent deformation was measured immediately after load release using the micrometer eyepiece of the microscope. Microindentations were performed starting in undeformed regions and proceeding in equidistant steps of 100–150 μm along the necking region into the cold drawn area. The hardness values (MPa) are calculated from the residual projected area of the indentation using the relation [22]

$$H = kP/d^2 \tag{1}$$

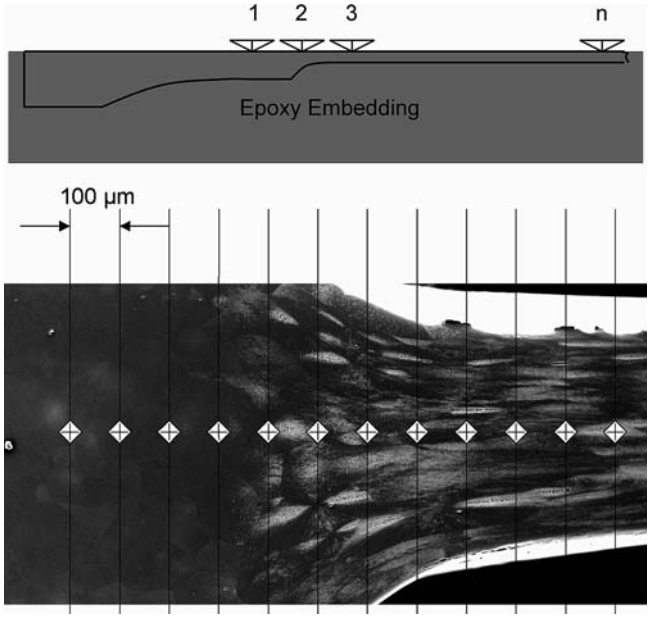

Fig. 2 Schematic representation of the sample embedded in epoxy resin, location of the indentations along the deformation axis and schematic representation of a row of indentations along the neck region for the α-iPP sample (SEM image after permanganic etching)

where d is the length (μm) of the impression diagonal, P is the load (N) applied and k is a geometrical factor equal to 1.854×10^6. The hardness values were derived from the indentation diagonals parallel $H_{||}$ and normal $H_{\perp}$ to the straining direction. Every data point represents the average of at least four indentations. The indentation anisotropy was calculated using the equation

$$\Delta H = \frac{H_{||} - H_{\perp}}{H_{||}} = 1 - \left(\frac{d_{||}}{d_{\perp}}\right)^2 \tag{2}$$

Scanning electron microscopy

Scanning electron microscopy was performed to locate the single indentations along the scan axis. A modified permanganic etching technique was applied to reveal the nanostructure of the deformed material [32]. Thus, the micromechanical events in the regions of interest can be correlated to the single indentations. In these regions representing typical states of deformation, micrographs of the deformation structures were recorded with a JEOL JSM 6300 SEM operated at 15 kV accelerating voltage. For the evaluation of the local strain at given distances, the deformation of spherulitic structures was measured from SEM micrographs using an ANALYSIS image analyser. For each data point, the average value of the diameter of, at least, ten spherulites in the axis parallel to the straining direction was evaluated.

Results

Microhardness H of the undeformed material

Table 1 collects the yield stress and the hardness values derived from the indentations in the undeformed areas of the PP samples presenting the two polymorphic forms α and β. The initial hardness values for the undeformed α-iPP and β-iPP are 105 and 90 MPa, respectively. These microhardness values are in good agreement with data reported earlier [33]. Accordingly, the crystallinities can be estimated using the following equations:

$$H^{\alpha} = w_c^{\alpha} H_c^{\alpha} + (1 - w_c^{\alpha}) H_a \tag{3}$$

Table 1 Comparison of tensile yield stress, calculated hardness from Eq. 4 and experimental hardness values for both types of the undeformed PP material. The degree of crystallinity calculated from Eqs. 2 and 3 and the minimum values of microhardness are also given

PP type	Yield stress σ_y (MPa); [30, 31]	Calculated hardness (Eq. 5)	Initial hardness H_i (MPa)	Crystallinity after Eqs. 3 and 4	Min. hardness H_{min} (MPa)
α-iPP Daplen BE50	36	108	105	$w_c^{\alpha} = 0.66$	70
β-iPP Daplen BE60	30	90	90	$w_c^{\beta} = 0.67$	27

$$H^{\beta} = w_c^{\beta} H_c^{\beta} + (1 - w_c^{\beta}) H_a \quad (4)$$

where $H_a \approx 30$ MPa, $H_c{}^{\alpha} = 143$ MPa, $H_c{}^{\beta} = 119$ MPa are the hardness values for the amorphous phase and the pure crystals in the α and β modifications of PP, respectively. For the α and β materials, crystallinity degrees of $w_c{}^{\alpha} = 0.66$ and $w_c{}^{\beta} = 0.67$ were calculated.

For the undeformed polymers, the obtained hardness values are in good agreement with the tensile stress values at yield according to the Tabor relation

$$H = 3\,\sigma_y \quad (5)$$

(see Table 1) [22].

Strain-induced changes of microhardness

α-Isotactic polypropylene

Figure 3 illustrates the variation of H for the α-iPP along the deformation axis from the starting point of the undeformed material. The first indentations along the deformation axis do not show any deviation from the original hardness values. As the material starts to deform plastically, a clear decrease of the hardness sets in. The hardness values given in Fig. 3 were derived from the impression diagonals parallel and normal to the stretching direction (Fig. 2). At a distance of about 1.5 mm from the starting point a minimum H value of 70 MPa is detected. The H-minimum is reached at the end of the necking region of the α-iPP tensile bar. Macroscopically one observes a stress whitening in the same area. After the neck, indentation anisotropy develops and the hardness values ($H_{||}$ and $H_{\perp}$) gradually increase in the drawn region of the tensile bar, $H_{||}$ exceeding the original hardness values.

β-Isotactic polypropylene

Figure 4 shows the variation of the microhardness values for the β-iPP bar along the deformation axis. Here, at about 1.2 mm from the starting point H markedly

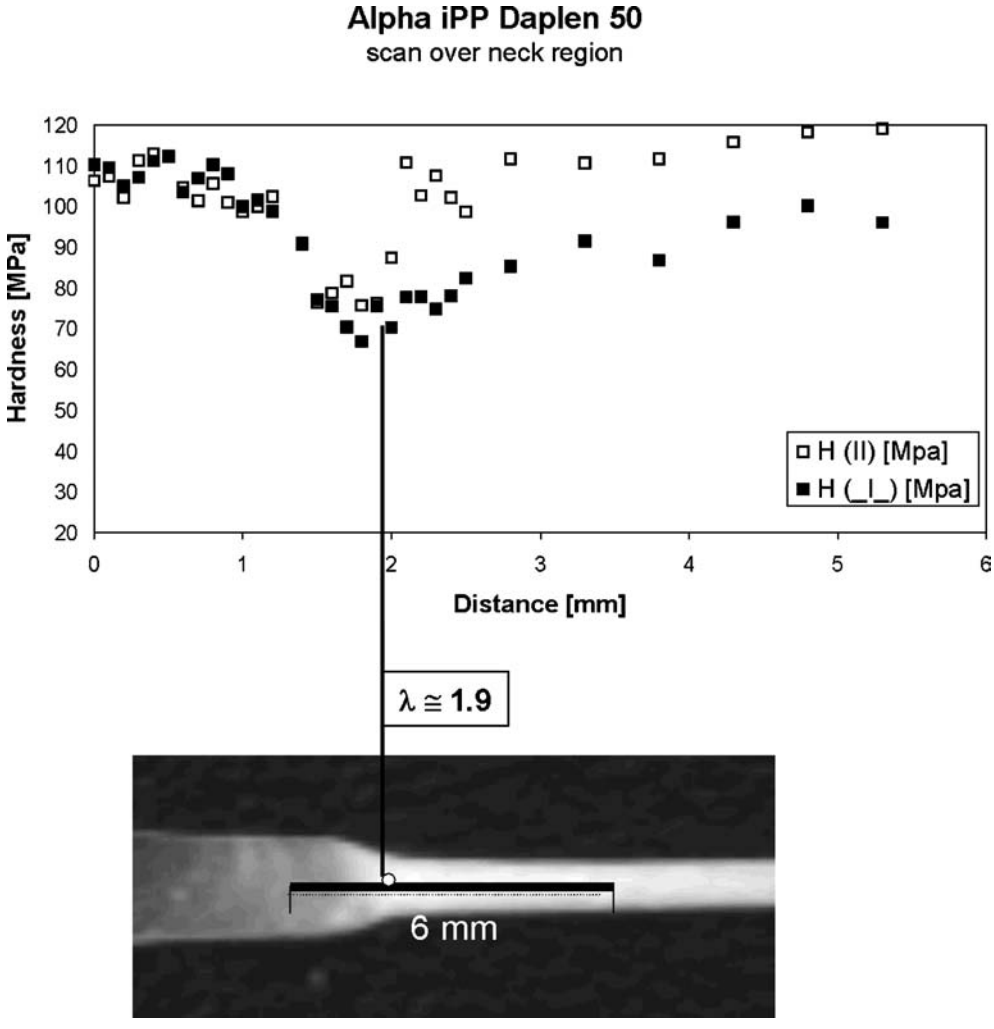

Fig. 3 Plot of H ($H_{||}$ and $H_{\perp}$) as a function of the distance from the undeformed end of the tensile bar (α-iPP). The stress whitening zone approximately starts at 1.5 mm

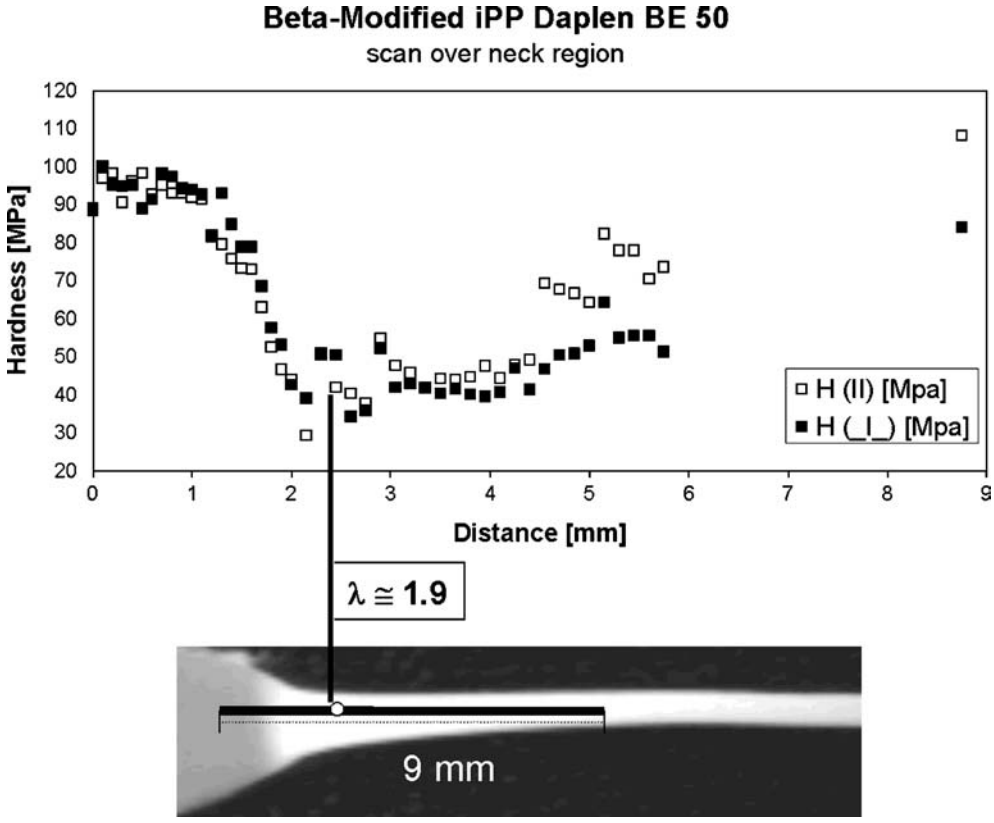

Fig. 4 Plot of H ($H_{||}$ and $H_{\perp}$) as a function of the distance from the undeformed end of the tensile bar (β-iPP). The stress whitening zone starts approximately at a distance of 1.5 mm

decreases, reaching a minimum of 27 MPa. Thereafter, the hardness increases along the deformation axis, in a similar manner to that observed for the α-iPP sample. For larger deformation values (distance $d = 9$ mm) the hardness $H_{||}$ exceeds again the original value for the undeformed material. In Fig. 5, the decrease of the microhardness $H_{||}$ is plotted against the local draw ratio λ (longest axis of single spherulites compared to the original average spherulite diameter of the undeformed material). As soon as a deformation of the spherulites is detected ($\lambda > 1$ at about 1.2 mm from the starting point) H linearly decreases reaching a minimum at $\lambda \approx 1.8$.

Indentation anisotropy

Figure 6 shows the variation of the indentation anisotropy calculated from the impression diagonals normal and parallel to the straining direction with increasing deformation along the deformation axis for α-iPP. For the initial stages of deformation ($\lambda \leq 2$) no anisotropy of the impression diagonals is observed. After the hardness minimum, a significant increase of the anisotropy occurs. At a distance $d = 1.7$ mm from the starting point (representing the necking region) the anisotropy starts to deviate from zero reaching an average of 25%, that remains constant for d-values along the cold drawn region of the tensile bar larger than 2 mm.

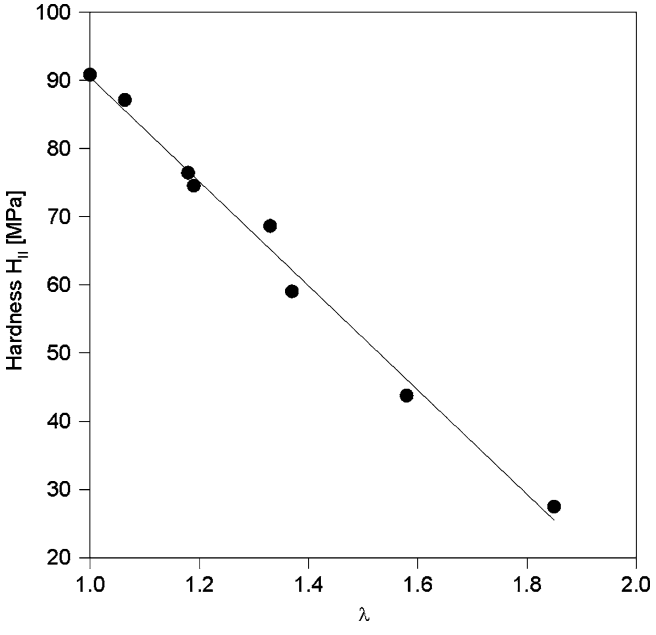

Fig. 5 Plot of $H_{||}$ for β-iPP against local elongation λ calculated from the deformation of the spherulitic structures at the loci of indentation

In the case of the β-iPP bar, after the hardness minimum at $d = 2.2$ mm the development of anisotropy is also observed (Fig. 7). The indentation anisotropy starts

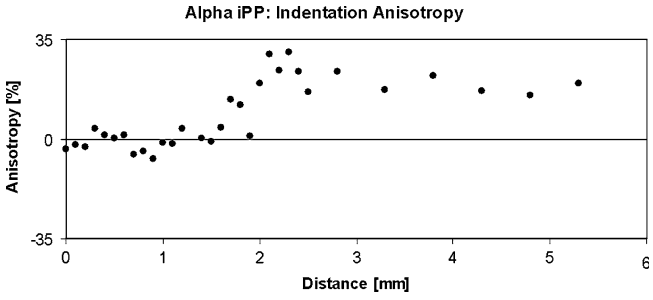

Fig. 6 Variation of indentation anisotropy for α-iPP along the deformation direction

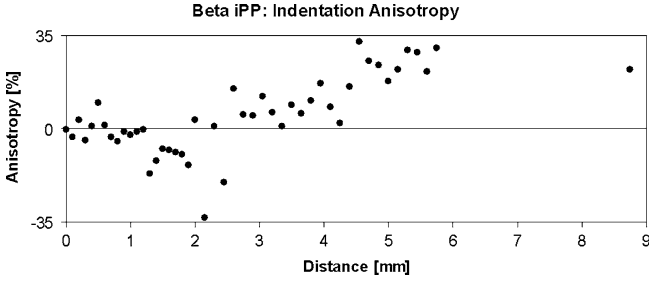

Fig. 7 Variation of indentation anisotropy for β-iPP along the deformation direction

to deviate from zero as soon as the microhardness starts to increase reaching a value of about 30%.

Strain-induced changes of morphology

The main differences between the spherulitic structures of the two types of iPP are illustrated in Fig. 8. The lamellae of the α-iPP grow radially from the centre of the spherulite (Fig. 8a). A typical feature of this nanostructure is the cross-hatched arrangement of the main lamellae and daughter lamellae forming a dense, mesh-like pattern (Fig. 8c). In contrast, the β-iPP lamellae grow in a sheaf-like manner that is distinguished by the overlay in Fig. 8b. The lamellae are arranged as stacks of lamellae running parallel to each other (Fig. 8d).

The changes in the morphology that are produced by uniaxial tensile deformation are illustrated for the β-iPP (Figs. 9, 10, 11 and 12). The initial stage of plastic deformation is characterized by two micromechanical mechanisms: (a) the formation of the so-called Chevron patterns due to a breaking and collective twisting of lamellar stacks. Such a mechanism of formation of Chevron fibres-like structures has also been found in the initial stages of deformation of HDPE [34]. (b) lamellar separation processes in an embryonic state. The former process can be interpreted as a collective twisting of bundles of lamellae nearly without microvoid formation or fibrillation. The latter process includes the formation of microvoids and fibrillation. Lamellar separation is dominated by the deformation of the interlamellar, amorphous material. In Figs. 9 and 10, the structures observed at elongations of $\lambda \approx 1.2$ and $\lambda \approx 1.3$, respectively, are given. In this case, the orientation of the lamellae was perpendicular to the straining direction. As the deformation process proceeds ($\lambda \approx 1.2$), the fibrils break, and larger microcracks occur (Fig. 11). At $\lambda \approx 2$, the original spherulitic structure is almost completely destroyed. The material has a microporous structure (Fig. 12). In contrast to α-iPP, in the β-iPP case the whole sample area contributes to micromechanical processes that are related to microvoid formation and nanofibrillation [35]. In the case of the β-modification of iPP, the observed microvoiding phenomena were not limited to specific regions within a single spherulite (polar or equatorial regions with respect to the straining direction).

These results are supported by transmission electron microscopic (TEM) observations that were recorded from RuO_4-stained ultrathin sections from similar regions of the tensile bar that are presented elsewhere [35]. Comparison of the results from the SEM observation of etched samples with the TEM images from the same area excludes the possibility to ascribe the observed structural changes to artefacts introduced by the etching technique.

Discussion

First stages of plastic deformation

Detailed information about the local deformation behaviour is shown in Fig. 5 by plotting the $H_{||}$ data for β-iPP against the local draw ratio λ. In the deformation range from $\lambda = 1$ to $\lambda = 1.8$, the microhardness decreases linearly with the elongation ratio. To understand this type of behaviour, it is convenient to consider the changes in the semicrystalline morphology for β-iPP at the spots of indentation. In Fig. 9, the morphology of the β-iPP material at a local elongation ratio of 1.2 shows the appearance of some micropores and the correlated hardness value decreases by about 10%. With increasing deformation the process of lamellar separation starts to become the dominating mode of plastic deformation (Fig. 10). The lamellar separation process involves a significant microvoid formation and fibrillation within the interlamellar, amorphous material. At this stage a large number of micropores is formed entailing relatively large sample volumes. As a consequence, the hardness starts to drop significantly. Figure 11 illustrates the formation of microcracks originating from craze-like structures within the amorphous portion. At a draw ratio $\lambda \approx 2$ the occurrence of a conspicuous microporous structure (Fig. 12) can be correlated with the lowest $H_{||}$ value shown in Fig. 5.

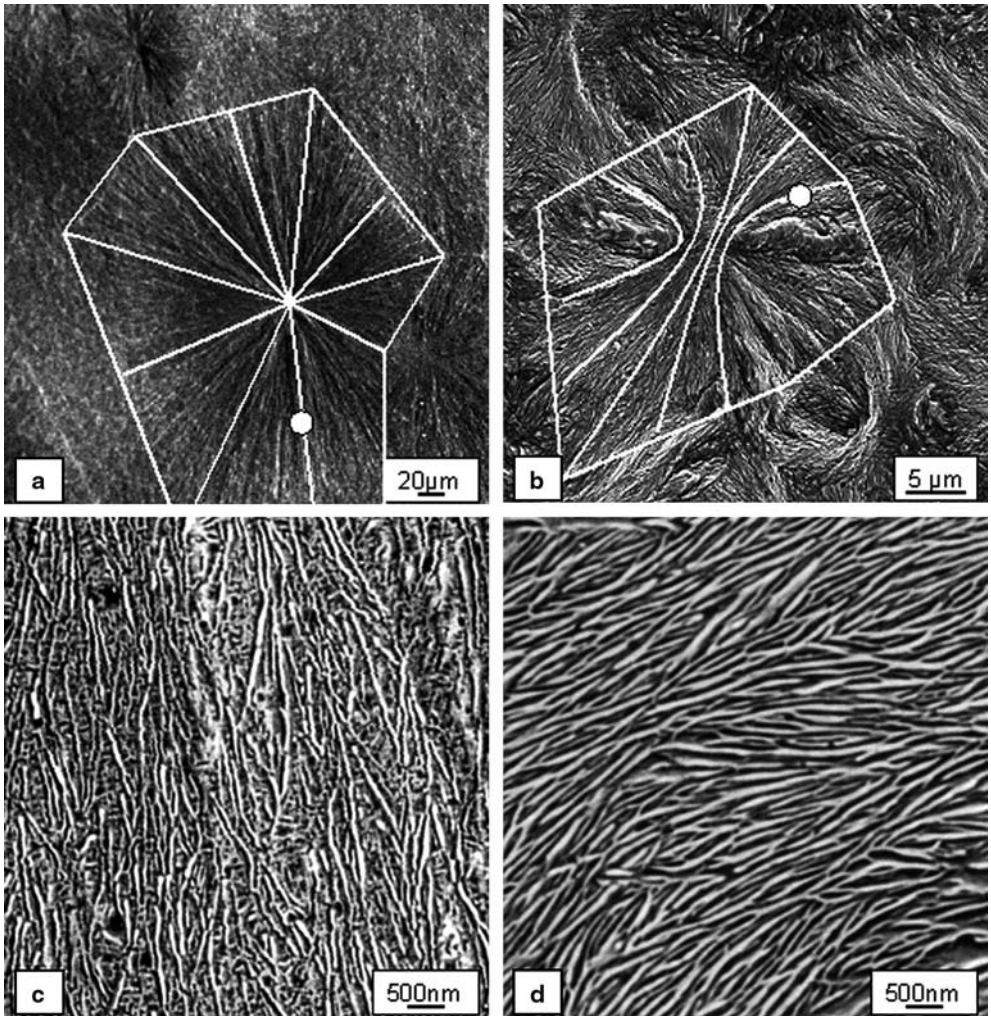

Fig. 8 Comparison of the original morphologies for α-iPP (**a, c**) and β-iPP (**b, d**) (undeformed material, SEM images after permanganic etching)

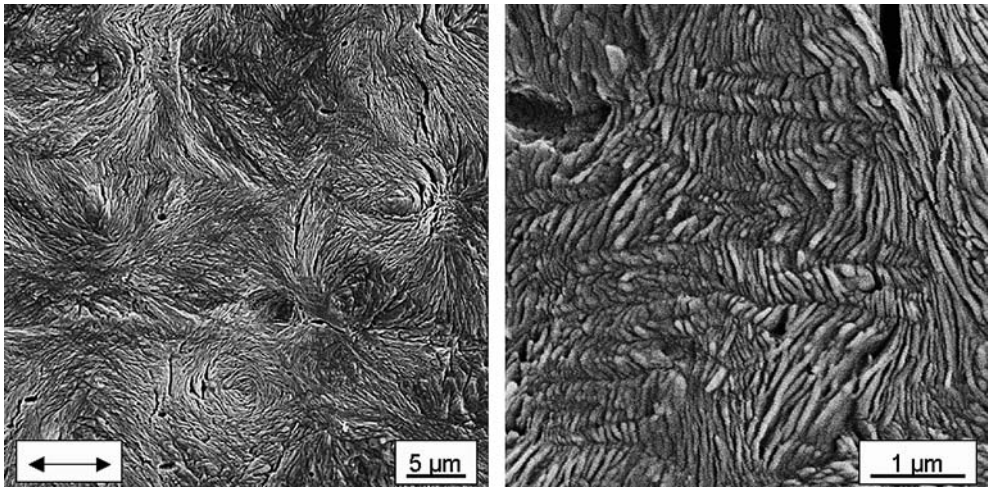

Fig. 9 Morphology of the deformed β-iPP sample at a distance of 1.2 mm from the undeformed end of the tensile bar ($\lambda \approx 1.2$, SEM images after permanganic etching). The deformation direction is indicated by an *arrow*

For higher draw ratios ($\lambda > 2$) the microhardness increases with increasing λ. At the maximum draw ratio reached in these experiments ($\lambda \approx 5$) $H_{||}$ exceeds the initial value of 90 MPa, levelling off to a value $H_{||} \approx 105$ Mpa, which is similar to the initial hardness of the neat α-iPP.

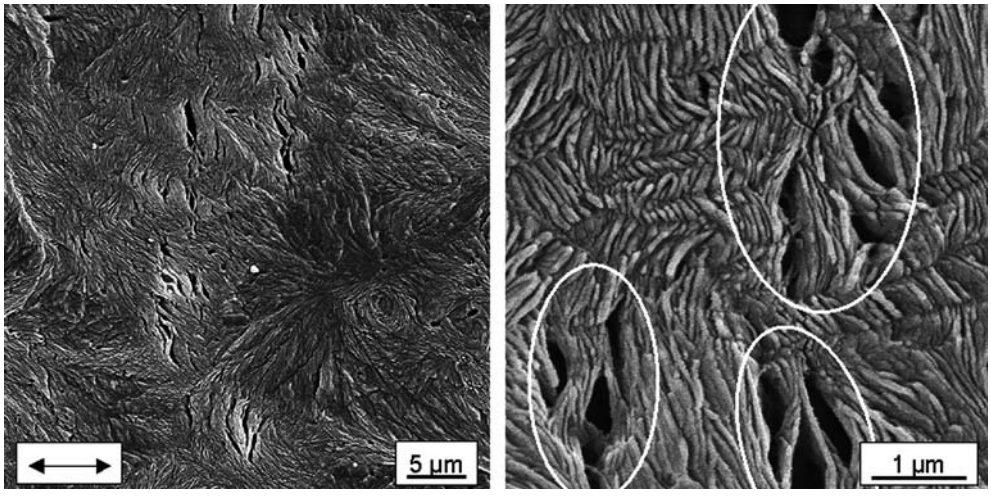

Fig. 10 Morphology of the deformed β-iPP sample at a distance of 1.4 mm from the undeformed end of the tensile bar ($\lambda \approx 1.3$, SEM images after permanganic etching)

At elongations near $\lambda = 2$ a steep drop in the microhardness for both, α- and β-iPP, is observed. The effect is more pronounced for the β modification. By inspection of the semicrystalline structures after deformation, one observes a prominent microvoid formation showing craze-like deformation processes, lamellar separation and intensive fibrillation (Fig. 11). The main difference between the neat α- and the β-iPP is that the spherulites of the β-iPP deform homogeneously, whereas the spherulites in the α-iPP only partially contribute to the elongation. Thus, the sample volume contributing to microvoid formation is significantly higher for the β-iPP.

Higher draw ratios and indentation anisotropy

After passing through a hardness minimum, the H values gradually increase exceeding the original hardness of the materials in both cases. Furthermore, $H_{||}$ increases faster than $H_{\perp}$ reaching a higher final value. Microindentation anisotropy has been reported for high strains in PE [27]. The anisotropic shape of the residual indentation can be attributed to the formation of a microfibrillar structure. The higher $H_{||}$ value derived from the indentation diagonal parallel to the fibre axis corresponds to an instant elastic recovery of the fibrous network in the drawn direction, whereas the lower $H_{\perp}$ value deduced from the diagonal perpendicular to the fibre axis defines the plastic component of the material [22]. The present experiments with PP show a similar process occurring at the early stages of deformation. By examining samples with higher λ, comparable to those reported for PE, both, an increase in hardness ($H_{||}$) and of anisotropy should be expected. This is the object of the present studies in our laboratories.

It is to be noted that the samples with the lowest microhardness values define the maximum level of porosity (at $\lambda \approx 2$). Furthermore, the maximum pore content at $\lambda \approx 2$ is in agreement with the draw ratio reported for microporous films of β modified PP having the highest porosity

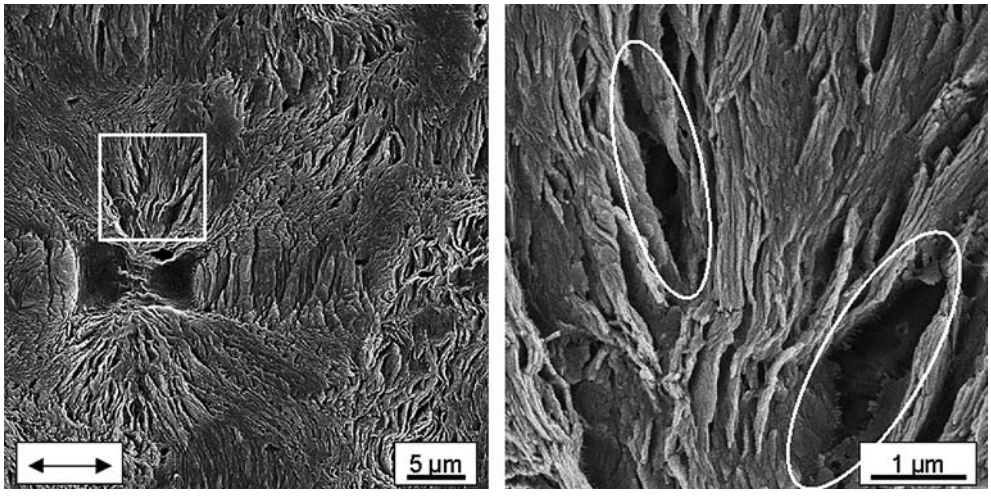

Fig. 11 Morphology of the deformed β-iPP sample at a distance of 1.7 mm from the undeformed end of the tensile bar ($\lambda \approx 1.4$, SEM images after permanganic etching)

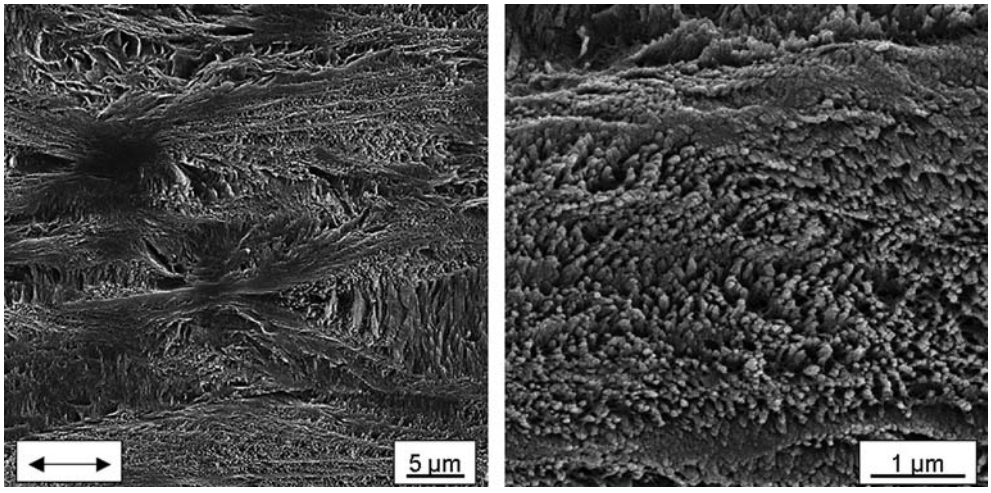

Fig. 12 Morphology of the deformed β-iPP sample at a distance of 2.6 mm from the undeformed end of the tensile bar ($\lambda \approx 2$, SEM image after permanganic etching)

of 39% [21]. As cold drawing proceeds, the pores start to close owing to the contraction of the sample in the direction normal to the straining direction and are transformed into gaps between the microfibrils of the highly oriented material. In agreement with experimental findings in Ref. [21], the porosity levels off with increasing draw ratio, at a value of $\lambda \approx 2.7$.

After surpassing the hardness minimum, one observes that strain hardening favours the increase of both microhardness and anisotropy. In the deformed samples the microhardness reaches larger values than in the undeformed material. This means that the effect of micropores ($H = 0$) is overcompensated by the orientation of microfibrils within the material. This effect is similar to the large hardness values found inside the crazes (containing micropores and fibrils) in amorphous polymers [24]. Studies on the quantitative correlation between microhardness and porosity are underway.

Conclusions

1. It was found that the microhardness of both, α- and β-iPP with increasing draw ratio shows a parallel drop with the localized transformation from the original spherulitic morphology into the fibre structure.
2. The drastic decrease of microhardness in the neck region can be explained in terms of nanomechanical processes involving lamellar separation, fibrillation and microvoid formation. This effect is more pronounced for the β- than for the α-modification of iPP.
3. The final anisotropic fibre structure yields a conspicuous indentation anisotropy that can be explained on the basis of an elastic recovery of microfibrils parallel to the fibre axis.

Acknowledgements We thank the Deutsche Forschungsgemeinschaft and the Kultusministerium des Landes Sachsen-Anhalt and MEC, Spain (grant FIS 2004-01331) for the support of this work. The financial support from the Deutscher Akademischer Austauschdient (DAAD) and from the Alexander von Humboldt-Stiftung is gratefully acknowledged. One of us (G.H.M.) thanks the Dirección General de Universidades, Ministerio de Educación, Spain, for the award of the Humboldt-Mutis Prize. S. Henning acknowledges a research scholarship from the Max-Buchner-Forschungsstiftung (MBFSt 2280) of the DECHEMA. Prof. J. Karger-Kocsis is thanked for the cooperation and supply of the materials.

References

1. Moore EP (1996) Polypropylene handbook. Hanser Verlag, Munich
2. Karger-Kocsis J (ed) (1995) Polypropylene: structure, blends and composites, vol 1. Structure and morphology. Chapman and Hall, London
3. Karian HG (ed) (1999) Handbook of polypropylene and polypropylene composites. Marcel Dekker, New York
4. Michler GH (1992) Kunststoff-Mikromechanik: morphologie, deformations—und Bruchmechanismen. Hanser, München
5. Peterlin A (1975) Colloid Polym Sci 253:809
6. Varga J (2002) J Macromol Sci Phys B 41(4–6):1121
7. Kausch HH, Plummer CJG (2001) Encyclopedia of materials: science and technology. Elsevier, Amsterdam
8. Baltá Calleja FJ, Peterlin A (1970) J Macromol Sci Phys B 4(3):519
9. Huang MR, Li XG, Fang BR (1995) J Appl Polym Sci 56:1323
10. Fujiyama M (1999) Intern Polym Processing 14:75
11. Turner Jones A, Aizlewood JM, Beckett DR (1964) Makromol Chem 75:134
12. Riekel C, Karger-Kocsis J (1999) Polymer 40:541
13. Karger-Kocsis J (1996) Polym Bull 36:119

14. Grein C, Plummer CJG, Kausch HH, Germain Y, Béguelin P (2002) Polymer 43:3279
15. Chen HB, Karger-Kocsis J, Wu JS, Varga J (2002) Polymer 43:6505
16. Tjong SC, Shen JS, Li RKY (1996) Polym Eng Sci 36:100
17. Dijkstra PTS, van Dijk DJ, Huétnik J (2002) Polym Eng Sci 42:152
18. Aboulfaraj M, G'Sell C, Ulrich B, Dahoun A (1995) Polymer 731–742
19. Li JX, Cheung WL, Chan CM (1999) Polymer 40:3641
20. Yoshida T, Fujiwara Y, Asano T (1983) Polymer 24:925
21. Chu F, Yamaoka T, Kimura Y (1994) Polymer 35:3442
22. Baltá Calleja FJ, Fakirov S (2000) Microhardness of polymers. Cambridge University Press, Cambridge
23. Baltá Calleja FJ In: Cunha AM, Fakirov S (eds) Structure development during polymer processing. Kluwer, Dordrecht pp 145–162
24. Michler GH, Ensslen M, Baltá-Calleja FJ, Könczöl L, Döll W (1999) Phil Mag A 79:167
25. García Gutiérrez MC, Michler GH, Henning S, Schade C (2001) J Macromol Sci Phys B 40:797
26. Baltá Calleja FJ, Giri L, Ezquerra TA, Fakirov S, Roslaniec Z (1997) J Macromol Sci Phys B 36:655
27. Baltá Calleja FJ (1976) Colloid Polym Sci 254:258
28. Flores A, Baltá Calleja FJ, Basset DC (1999) J Polym Sci Polym Phys 37:3151
29. Krumova M, Karger-Kocsis J, Baltá Calleja FJ, Fakirov S (1999) J Mater Sci 34:2371
30. Borealis data sheet P1078 07.06.2001 Ed. 1, http://www.borealisgroup.com/public/customer/data_sheets/Data_sheets.jsp
31. Borealis data sheet P0932 10.01.2002 Ed. 5, http://www.borealisgroup.com/public/customer/data_sheets/Data_sheets.jsp
32. Olley R, Bassett DC, Hine PJ, Ward IM (1993) J Mater Sci 28:1107
33. Baltá Calleja FJ, Martínez Salazar J, Asano T (1988) J Mater Sci Lett 7:165
34. Michler GH (1992) Colloid Polym Sci 270:627
35. Henning S, Adhikari R, Michler GH, Baltá Calleja FJ, Karger-Kocsis J (2004) Macromol Symp 214:157–171